THE JOURNAL OF PHYSICAL CHEMISTRY B

Article

pubs.acs.org/JPCB

# Structure–Property Relationships in Amorphous Microporous Polymers

Satyanarayana Bonakala and Sundaram Balasubramanian*

Chemistry and Physics of Materials Unit, Jawaharlal Nehru Centre for Advanced Scientific Research, Bangalore 560 064, India

Supporting Information

**ABSTRACT:** Structural models and physical properties of several amorphous microporous polymers (AMPs) have been investigated using molecular dynamics simulations in an all-atom framework. The modeled structures of AMPs are quantitatively consistent with experimental observations. A linear relationship between the accessible surface area (ASA) and mass density of AMPs has been established. In the AMP network constituted by planar nodes, near-neighbor nodes are oriented parallel to each other. The microporous structural models are further validated by the calculation of $CO_2$ and $N_2$ adsorption isotherms at 298 and 77 K, respectively, obtained through Grand Canonical Monte Carlo (GCMC) simulations. The isotherms and isosteric heat of adsorption computed within a force field approach are able to well reproduce the experimental results. The nature of interactions between the functional groups of the AMPs framework and $CO_2$ have been identified. An excellent $CO_2$ uptake with high heat of adsorption has been observed in AMPs containing nitrogen-rich building blocks.

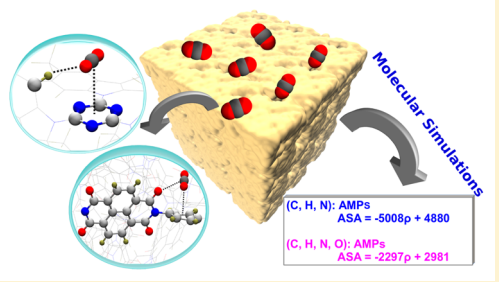


## 1. INTRODUCTION

Porous organic polymers have attracted considerable research interest due to their fine-tuned microporosity, large surface area,[1−3] and good stability.[4−8] Several porous organic polymers are envisaged as potential materials for the storage and separation of gases such as $CO_2$,[9−18] $H_2$,[19−25] and $CH_4$[26−28] as well as for the adsorption of organic solvents.[29] They include crystalline covalent organic frameworks (COF)[30−33] and amorphous microporous polymers (AMP) such as polymers of intrinsic microporosity (PIM),[34−37] conjugated microporous polymers (CMP),[38−40] and porous aromatic frameworks (PAF).[41,42] In general, AMPs are kinetically controlled products[43] and do not show long-range periodic order in their structure. Their amorphous nature offers a wide and vital scope for molecular simulations.[44−46] Simulations can provide useful insights into the molecular-level structure,[47−49] organization, and gas adsorption processes[41,50] in a manner that is complementary to experimental techniques. Ideally, they can also provide a rationale to understand the structure−property relationship in AMPs. It is in this spirit that we approach the problem herein.

Density is one of the important physicochemical parameter in polymer manufacturing process. In CMPs, it is useful to have prior knowledge of the density of polymer material in order to synthesize potential candidates for the removal of oil spills.[51−54] To our knowledge, the density of none of the AMPs has been reported experimentally so far in the literature, likely due to their porous nature. In the present work, we provide an empirical relationship between the accessible surface area of an AMP and its density. As the former can be experimentally determined, this relation could be potentially used to obtain an estimate of the density of the sample. In pursuit of this aim, employing MD simulations, we have arrived at atomistic models of several AMPs whose synthesis and property characterization have been reported in the literature. All the AMPs considered here possess nodes and linkers which are $\pi$-electron-rich and may additionally contain nitrogen-rich molecular groups. The extended conjugation and $CO_2$-philic nature of these moieties enable these polymers for $CO_2$ sorption. Our structural models are quantitatively validated against experimental properties. In particular, Grand Canonical Monte Carlo simulations were carried out to obtain $CO_2$ and $N_2$ adsorption isotherms. Predictions of adsorption isotherms of $CO_2$ in various AMPs for which experimental data have not yet been reported are also made. From a microscopic perspective, the following interactions between the polymer framework and $CO_2$ were found to be vital: (i) hydrogen bonding between O of $CO_2$ and H of pyrrole N−H or carbazole C−H, (ii) $\pi$−$\pi$ interaction of $CO_2$ with triazine or phenyl rings, and (iii) Lewis acid−base interaction between C of $CO_2$ and O of C═O groups.

## 2. RESULTS AND DISCUSSION

**2.1. Structural Properties.** MD simulations using an empirical force field were carried out on model AMPs. The schematic representations of monomeric and oligomeric units of various AMPs which have been considered in our simulations are shown in Figure 1. Details of these simulations,

**Received:** September 10, 2015
**Revised:** December 28, 2015
**Published:** January 4, 2016





DOI: 10.1021/acs.jpcb.5b08842
J. Phys. Chem. B 2016, 120, 557−565

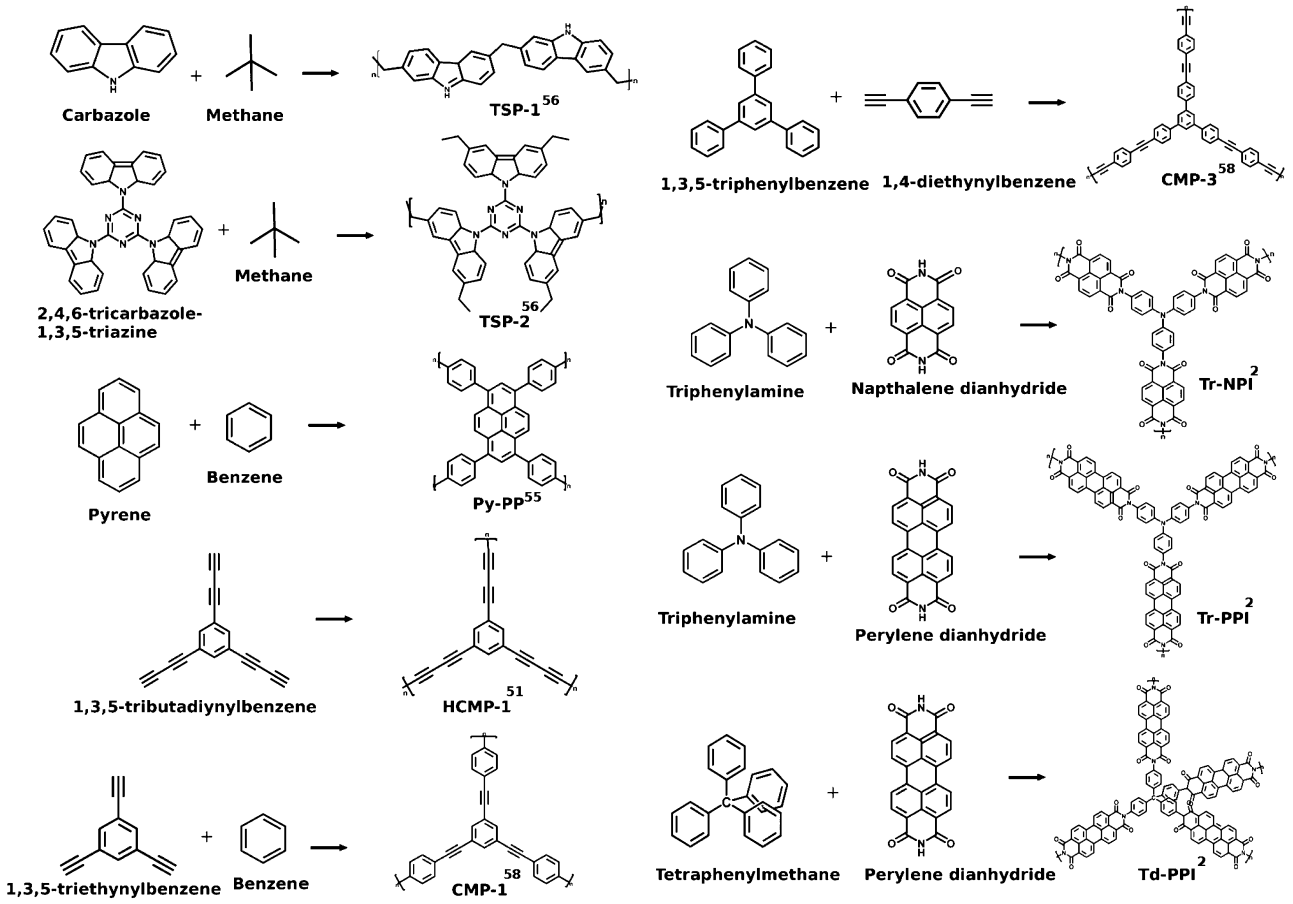


**Figure 1.** Schematic representations of monomeric and oligomeric units of various AMPs. Superscripts denote the reference in which the experimental synthesis and characterization of the compounds are described.

protocols, and interaction potentials are provided in the Supporting Information. The modeled structures of Py-PP,[55] TSP-2,[56] HCMP-1,[51] TPE-CMP,[57] CMP-1,[58] TSP-1,[56] CMP-3,[59] Tr-NPI,[2] Tr-PPI,[2] and Td-PPI[2] were characterized through calculations of (i) accessible surface area, (ii) powder X-ray diffraction pattern, and (iii) adsorption isotherms of $CO_2$. The quantity that is commonly studied to experimentally characterize the AMPs in terms of porosity is the surface area (calculated using the Brunauer−Emmett−Teller (BET) relation for $N_2$ sorption isotherm measured at 77 K[60]). It has been suggested that for crystalline solids the solvent accessible surface area (ASA) calculated using the Monte Carlo method is the most appropriate for a comparison to the experimentally determined BET surface area, rather than the geometric method (Connolly surface).[61] The validity of this equivalence has not been tested for amorphous porous solids yet. The appropriateness of this assumption has also been verified by us by calculating the BET surface area of all the AMPs[62] through the calculation of their $N_2$ adsorption isotherms obtained from GCMC simulations at 77 K. The results are presented later. However, in the following discussion, we employ ASA as a measure of porosity, as it is computationally easier to calculate than the BET surface area.

Many of the AMPs studied here have been simulated at different system sizes—varying both the number of nodes and number of linkers in an oligomer as well as by varying the number of oligomers in the simulation as well. Results from all these simulations are presented in the Supporting Information. Unless stated otherwise, the main text contains results from the smallest system size studied.

The accessible surface areas of model structures obtained from MD simulations were calculated using a Monte Carlo code developed by Snurr and co-workers.[63] A probe diameter value for $N_2$ of 3.681 Å was employed in these ASA calculations. As reported in our earlier study on tetraphenylethene-based conjugated microporous polymer, TPE-CMP,[57] equilibrium MD simulations indeed yield structures that are denser and less porous than that of the experimental sample. This is not unexpected as the simulations yield a structure which is thermodynamically controlled (and dense), although lacking in long-range periodicity, while the experimental sample is one which is likely to be kinetically controlled (depending on conditions of synthesis) and possessing large porosity. In order to obtain a ASA which is comparable to that of the experimental sample, the density of the model compound was decreased manually, in steps. At each step, post energy minimization, MD simulations in the constant NVT ensemble for over 2 ns were carried out, and subsequently the ASA was calculated. This process was continued until the calculated and experimental ASA values nearly matched. This procedure yields many model structures for each microporous polymer each with a different ASA. In principle, such structures for a particular compound constitute an ensemble which could represent experimental samples obtained under different synthetic conditions.[64,65] However, further analysis are carried out only on those models whose ASA are comparable to that of experimental sample. These values for different AMPs are tabulated in Table 1. The table also contains the percentage of


DOI: 10.1021/acs.jpcb.5b08842
J. Phys. Chem. B 2016, 120, 557−565

void volume in the modeled structures, which will be discussed later.

**Table 1. Comparison between Accessible Surface Area ($m^2$/g) of AMPs of Simulated Models and Experiment; Percentage of Void Space in the Model Structures Estimated Using Mercury[67]**

| AMP | ASA (simul) | $S_{BET}$ ($m^2$/g)[a] | ASA (expt) | % of void space |
|---|---|---|---|---|
| Td-PPI | 2198 | 2209 | 2213[2] | 78.0 |
| Py-PP | 1072 | 1071 | 1070[55] | 32.1 |
| TSP-2 | 911 | 919 | 913[56] | 31.0 |
| TPE-CMP | 852 | 853 | 854[57] | 23.1 |
| HCMP-1 | 843 | 845 | 842[51] | 22.9 |
| CMP-1 | 835 | 837 | 834[58] | 22.2 |
| TSP-1 | 561 | 567 | 563[56] | 21.1 |
| Tr-NPI | 575 | 579 | 567[2] | 19.6 |
| CMP-3 | 537 | 517 | 522[59] | 19.6 |
| Tr-PPI | 404 | 395 | 400[2] | 15.2 |

[a]Surface area calculated from $N_2$ adsorption isotherms (obtained through GCMC simulations with MCIN[71]) using the BET method.

How realistic are the structural models that possess the same ASA as that of experiment? The procedure adopted here to come up with porous structures of AMP was adopted earlier by us in the case of tetraphenylethene-based conjugated microporous polymer, TPE-CMP.[57] In that work, we had compared the powder X-ray diffraction pattern calculated for the structural model against the experimental result. The same was shown in Figure 3a of ref 57, and the comparison was excellent. Incidentally, the experimentally determined PXRD patterns of TSP-1,[56] TSP-2,[56] Td-PPI,[66] Tr-PPI,[66] Tr-NPI,[2] and Py-PP[55] are available. Thus, we compare powder X-ray diffraction (PXRD) patterns calculated for the model structures (whose ASA matches with the experimental value) using Mercury[67] against experimental data. Figure S11a–f exhibits the same, and again the match between experiment and theory is reasonable. We are unable to make similar comparisons for other AMPs as their experimental patterns are not available in the literature. On the basis of the good agreement in the powder patterns, we believe that the computed structural models for AMPs are reasonable representations of the experimental ones.

The ASA of several AMPs has been plotted against their mass densities in Figure 2 and Figure S10. To reiterate, only one data point per AMP corresponds to the ASA value reported experimentally; the same are indicated by plus symbols in Figure 2. These symbols can be fitted to a straight line. The fits suggest the following categorization of AMPs: (i) ones containing C, H, and N: HCMP-1, CMP-1, CMP-3, Py-PP, TPE-CMP, TSP-1, and TSP-2; (ii) AMPs containing C, H, N, and O atoms: Tr-NPI, Tr-PPI, and Td-PPI. The parameters of fit are $m = -5008$ $m^5/kg^2$, $c = 4880$ $m^2/g$ for AMPs without the C═O group and $m = -2297$ $m^5/kg^2$, $c = 2981$ $m^2/g$ for AMPs possessing the C═O group. Here, $m$ and $c$ are the slope and intercept of the best fit line. These relationships could be useful not only for synthetic and process chemists but also in molecular modeling. Density is a critical input for atomistic MD simulations. As the same is not determined experimentally, modellers can employ these expressions while setting up the AMP system of interest. It is also noteworthy that models of an AMP with ASA values other than that of experiment fall on the same line as the one connecting the experimental data points.

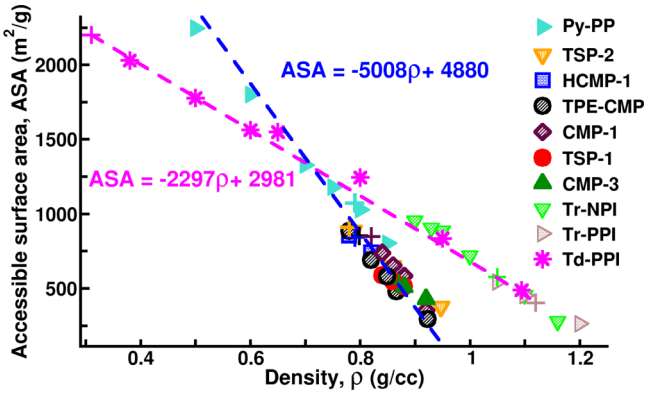


**Figure 2.** Correlation between the accessible surface area and density of various AMPs. Plus (+) symbols correspond to modeled AMPs possessing the experimentally measured accessible surface areas. Other symbols denote models of various AMPs obtained at different computational "synthetic" conditions. The invariance of the correlation with system size is demonstrated in Figure S10.

Among the few ways that the structure of AMPs can be characterized is the pair correlation function,[68] $g(r)$. These have been calculated between different molecular groups to understand the effect of building block arrangements on the ASA. Pair correlation functions (PCFs) between center of masses of nodes are shown in Figure 3.

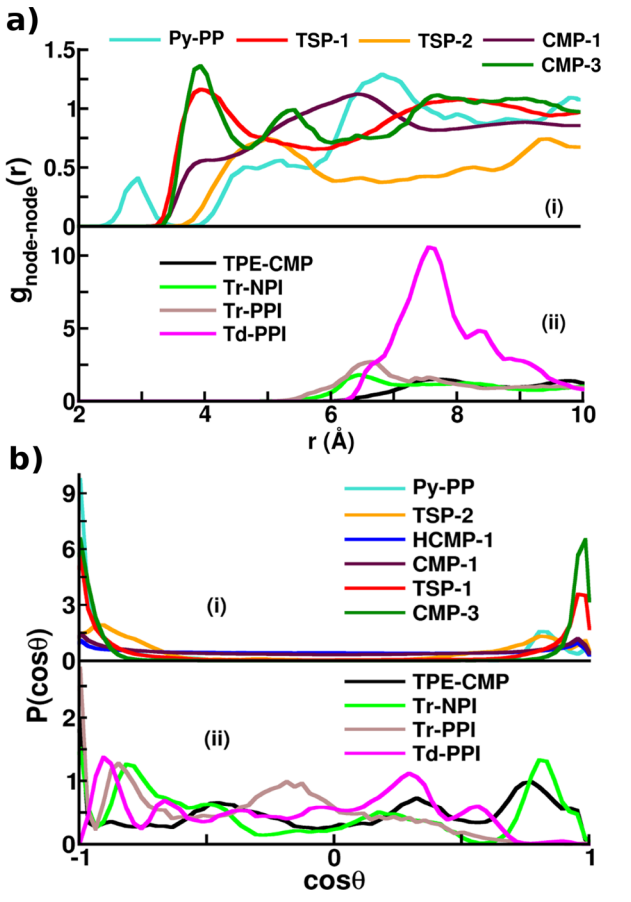


**Figure 3.** (a) Comparison of the intermolecular pair correlation functions between nodes of modeled AMPs and (b) Angle distribution of ring normals of near-neighbor nodes present within an oligomer in AMPs.



DOI: 10.1021/acs.jpcb.5b08842
J. Phys. Chem. B 2016, 120, 557–565

While the energy-minimized structures of the nodes of Tr-PPI and Tr-NPI are trigonal pyramidal, those of TPE-CMP[57] and Td-PPI are tetrahedral in their geometries. Such node structures allow the polymer network to grow three-dimensionally. The corresponding oligomer structures are shown in Figures S7–S9. The three-dimensional network topology causes the node–node distance in TPE-CMP, Tr-NPI, Tr-PPI, and Td-PPI to be larger than those of the other (largely two-dimensional) AMPs. The same is reflected in the position of the first peak of the node–node $g(r)$ in Figure 3a. From Figure 3a and Table 1, we can realize that the ASA of the microporous polymer increases with increase in the distance between nodes. The difference in the geometries of the monomers thus considerably influences ASA. For instance, the ASA of Td-PPI is larger than that of Tr-PPI, although both the networks have the same linker, perylene polyimide (PPI). The possibility of pyramidal inversion around the N-center in Tr-PPI induces the formation of hyperbranched networks compared to closed ring structures, as reported in the literature.[66,69] Therefore, this flexibility in the conformation of the building block in Tr-PPI has been recognized to hamper its surface area.[69] In the case of Td-PPI, the three-dimensional network is formed from the conformationally more rigid tetrahedral geometry of tetraphenylmethane. As a result, it forms a closely packed 3-D network, with higher surface area.[70] The height of the first peak in the node–node $g(r)$ of Td-PPI is larger than in Tr-PPI or Tr-NPI. This is due to the node rigidity in the former and the larger node–node distance.

In order to further characterize the structure of AMPs, the orientational order between neighboring nodes was calculated from the configurations obtained from MD simulations.[72] One set of AMPs shown in Figure 3b(i) possess neighboring nodes whose planes are oriented parallel to each other; however, the other set (Figure 3b(ii)), consisting of TPE-CMP, Tr-NPI, Tr-PPI, and Td-PPI, are structured in such a fashion that the ring planes of neighboring nodes are oriented in all possible directions, although a parallel orientation is marginally more preferred. It is to be noted that the nodes in the latter set are three-dimensional in nature while those in the former set are largely planar. The near-planarity of the nodes themselves make internode angles to be either 0 or 180°. As a consequence, the height of the first peak in the node–node $g(r)$ in AMPs with planar nodes is less than or comparable to unity; in the case of AMPs with nonplanar nodes, the $g(r)$ peaks are much taller, as can be seen from Figure 3a(ii).

The connectivity among the pores and void spaces in the modeled AMPs were obtained using $N_2$ with a probe radius of 1.82 Å through Mercury.[67] The same is shown in Figure 4. AMPs shown in Figure 4a–d,i,j possess large surface areas, and the voids are interconnected to each other in either two or three dimensions. However, the pore architecture in AMPs with lesser surface area (Figure 4e–h) is largely one-dimensional. The percentages of void volume of various AMPs are tabulated in Table 1. ASA is seen to increase with increase in the percentage of void space in polymer network.

**2.2. Adsorption Isotherms of $N_2$ and $CO_2$.** The adsorption isotherms of $N_2$ in different AMPs at 77 K were calculated using GCMC simulations.[71] These calculations were undertaken so as to compare against experimentally determined isotherms as well as to calculate their surface area using the Brunauer–Emmett–Teller (BET) method.[62] In particular, the plus symbol in the plot of ASA–density correlation in Figure 2 refer to the experimentally determined BET surface area, while the rest of the symbols refer to the solvent accessible surface area (ASA) calculated by us for the structural models simulated herein. Thus, in principle, one needs to show that, at least for the compounds studied here, the ASA matches the BET result. This too provides a compelling reason for us to calculate the $N_2$ isotherms for some of the AMPs.

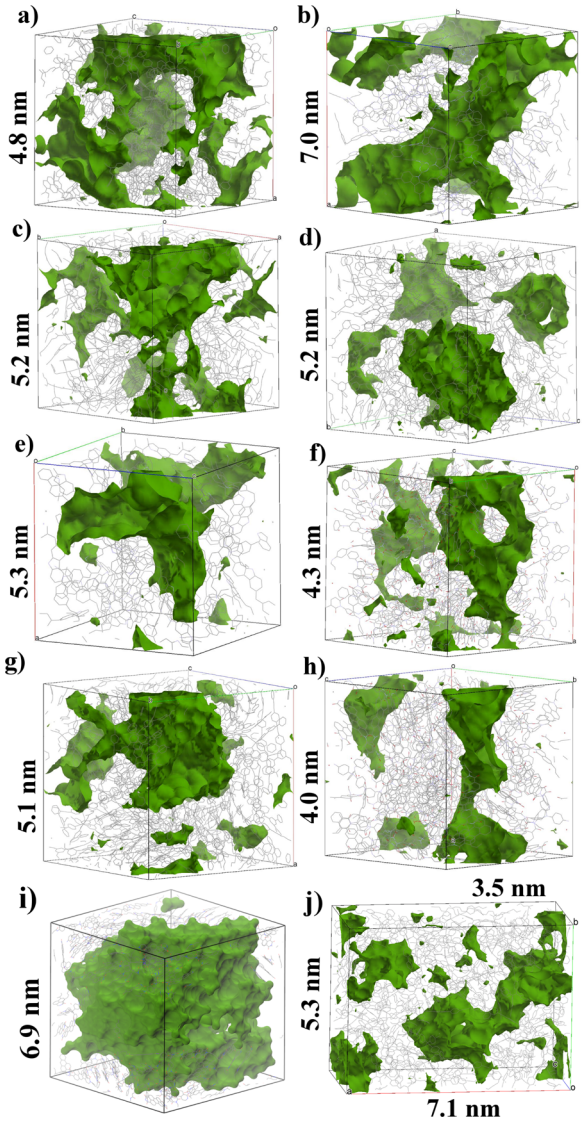


**Figure 4.** Pore architecture in the structural models of various AMPs determined through Mercury:[67] (a) Py-PP, (b) TSP-2, (c) HCMP-1, (d) CMP-1, (e) TSP-1, (f) Tr-NPI, (g) CMP-3, (h) Tr-PPI, (i) Td-PPI, and (j) TPE-CMP. The green region indicates voids for $N_2$ while atoms of the polymer are in line representation. Edges of the cubic simulation cell and its dimensions are mentioned.

The $N_2$ isotherms in TSP-1, TSP-2, and TPE-CMP were calculated up to $P/P_0$ = 1. However, to calculate the BET surface area, one needs only low pressure ($<P/P_0$ = 0.35) adsorption data.[62] Hence, we have calculated the amount of $N_2$ uptake up to $P/P_0$ = 0.2 for the remaining AMPs. The calculated isotherms are compared against experimental data in Figure 5. The surface areas of several AMPs which were obtained by applying BET model on the calculated $N_2$ adsorption isotherms at 77 K are tabulated in Table 1. The calculated BET surface areas ($S_{BET}$) compare well against the reported experimental values. This acts as a further validation of our modeled structures.



DOI: 10.1021/acs.jpcb.5b08842
J. Phys. Chem. B 2016, 120, 557–565

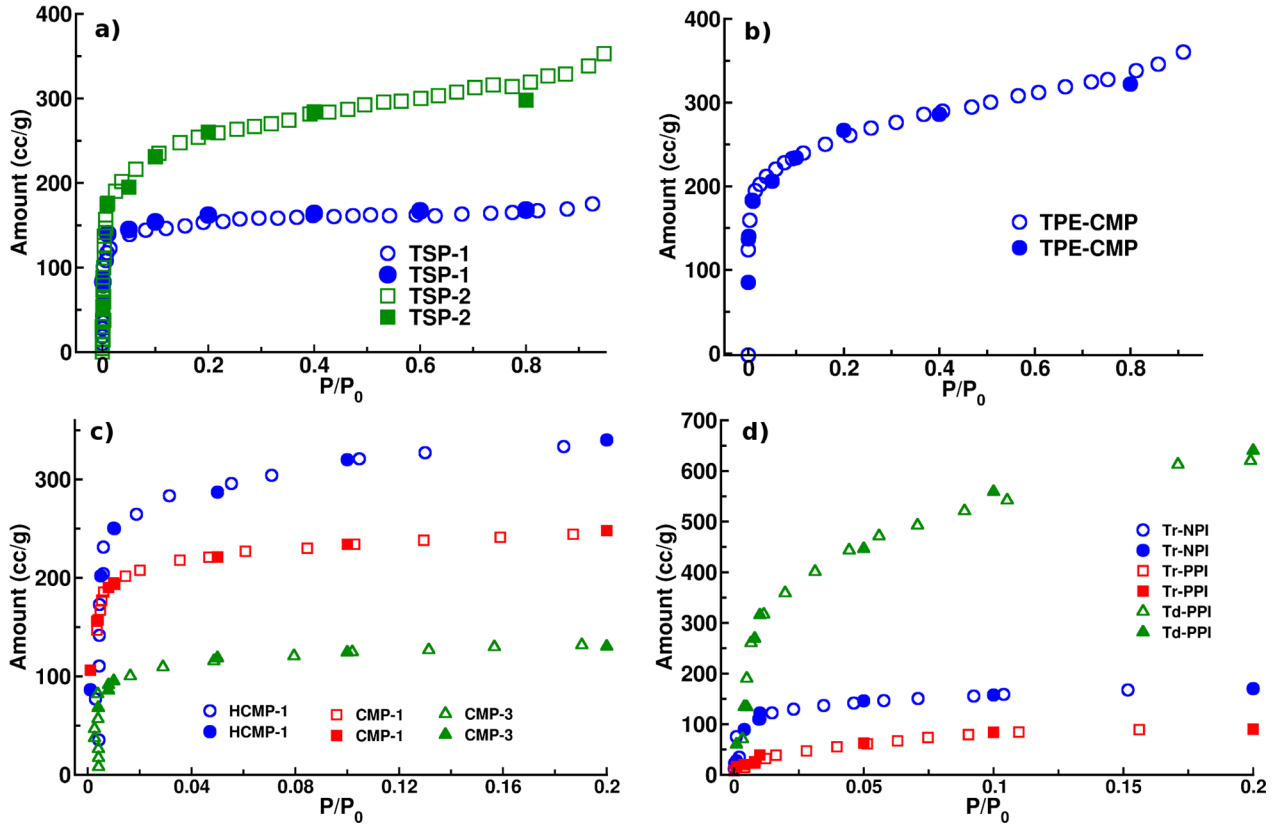


**Figure 5.** Comparison of adsorption isotherms at 77 K of $N_2$ in (a) TSP-1,[56] TSP-2,[56] (b) TPE-CMP,[57] (c) HCMP-1,[51] CMP-1,[58] and CMP-3,[59] and (d) Tr-NPI,[2] Tr-PPI,[2] and Td-PPI[2] calculated using MCIN code[71] (closed symbols) against experimentally measured data (open symbols) obtained from literature. References to experiments are provided in Table 1.

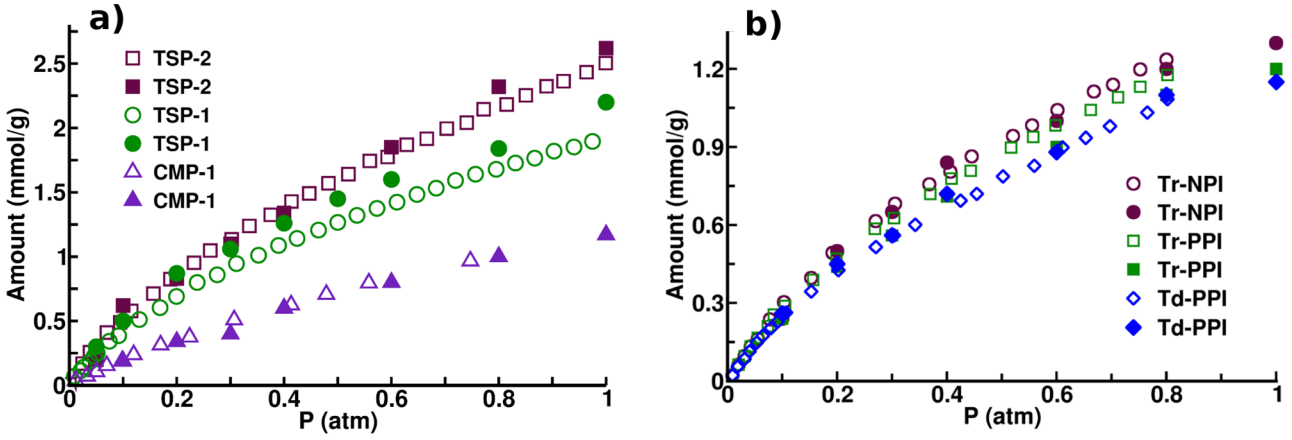


**Figure 6.** Comparison of adsorption isotherms at 298 K of $CO_2$ in (a) TSP-1,[56] TSP-2,[56] and CMP-1[58] and (b) Tr-NPI,[2] Tr-PPI,[2] and Td-PPI[2] calculated using MCIN code[71] (closed symbols) against experimentally measured data (open symbols).

Further, the adsorption isotherms of $CO_2$ in several AMPs at 298 K were obtained using GCMC simulations.[71] Experimental data are available in the literature for six of these compounds. TSP-1 and TSP-2 contain triazine and carbazole groups, respectively, and are considered to be bifunctionalized task-specific porous polymers with good surface area (562.5 and 913.0 $m^2/g$ for TSP-1 and TSP-2, respectively) and thermal stability (up to 800 °C). Because of the presence of $CO_2$-philic nitrogen-rich building blocks in the polymer frameworks, these materials exhibit excellent $CO_2$ uptake abilities.[73] In TSP-2, the maximum $CO_2$ storage can be up to 18.0 wt % at ambient conditions, which is more than that reported in other many porous organic polymers.[58,74−78] Computational results for TSP-1, TSP-2, Tr-NPI, Tr-PPI, Td-PPI, and CMP-1 are compared against experimental data in Figure 6a,b, and the comparison is rather good. Noticeably, $CO_2$ isotherms in CMP-1 (see Figure 6b) and in TPE-CMP (see Figure 4F of ref 57), which too do not contain any polar atom,[57] could be quantitatively reproduced without the inclusion of sorbent−sorbate electrostatics. GCMC simulations of $CO_2$ adsorption in AMPs without C═O, C═N, and N−H groups but modeled with Gasteiger charges on all the atoms yielded nearly identical adsorption isotherms as those carried out without sorbent−sorbate electrostatics. Hence, in the current paper, we adopted


DOI: 10.1021/acs.jpcb.5b08842
J. Phys. Chem. B 2016, 120, 557−565

the same procedure for calculating the $CO_2$ adsorption isotherms in the following AMPs: Py-PP, HCMP-1, and CMP-3, which too do not carry any polar atoms. The calculated $CO_2$ adsorption isotherms for all the AMPs are shown in Figure 7. TSP-2 exhibits the maximum uptake of $CO_2$ at ambient conditions.

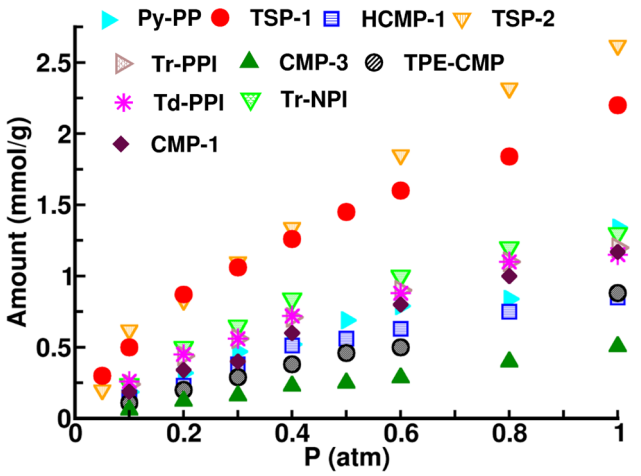


**Figure 7.** Adsorption isotherms of $CO_2$ in several AMPs at 298 K calculated using GCMC simulations.

The remarkable agreement between the isotherms determined through experiments and by simulations further reinforces the idea that the model structures are representative of the compounds. The models have been further validated by a comparison of the isosteric heat of adsorption ($Q_{st}$) for $CO_2$ against experimental results. $Q_{st}$ was computed from the fluctuations in the number of particles and in the total energy[79] from the GCMC run at low pressures as follows:

$$Q_{st} = RT - \frac{\langle UN\rangle - \langle U\rangle\langle N\rangle}{\langle N^2\rangle - \langle N\rangle^2} \quad (1)$$

where $U$ is the total energy, and $N$ is the number of adsorbed molecules, and the angular brackets denote ensemble averages.

$Q_{st}$ values for $CO_2$ at 0.05 atm in TSP-1 and TSP-2 have been calculated to be 28.6 and 31.0 kJ/mol, respectively. These values are in good agreement with the experimentally obtained zero coverage isosteric heat of adsorption for $CO_2$ in TSP-1 and TSP-2, which are 28.1 and 30.3 kJ/mol,[56] respectively. In addition, $Q_{st}$ for $CO_2$ in Tr-NPI, Tr-PPI, and Td-PPI obtained at 0.1 atm are tabulated in Table 2. The table also provides the experimentally determined heats of adsorption wherever available. Figure 7 and Table 2 suggest that AMPs consisting nitrogen-rich building blocks exhibit excellent $CO_2$ uptake ability with significant heat of adsorption.

The remarkably high heats of adsorption can be understood in terms of $CO_2$ interactions with specific functional groups of the AMP. To understand these, we have examined several configurations of the adsorbed gas obtained from GCMC simulations at low pressures. Possible interactions between $CO_2$ and TSP-1, TSP-2, HCMP-1, and Tr-NPI identified from the GCMC simulations are shown in Figure 8. $CO_2$ is seen to be involved in (i) hydrogen bonding between H of pyrrole N−H and carbazole C−H and O of $CO_2$, (ii) $\pi-\pi$ interaction with triazine ring and phenyl moieties, and (iii) Lewis acid−base interactions with the O of napthalene dianhydride's C═O group and C of $CO_2$. Given the absence of electronic degrees of freedom in our simulations, these interactions have been identified on established geometric criteria alone.[80−83]

**Table 2. Comparison between Isosteric Heat of Adsorption ($Q_{st}$ (kJ/mol)) Values of $CO_2$ Calculated from GCMC Simulations via Eq 1 and Experimental Data in Various AMPs**

| AMP | simulation (kJ/mol) | experiment (kJ/mol) |
|---|---|---|
| Td-PPI | 20.1 | |
| Py-PP | 23.4 | |
| TSP-2 | 30.9 | 30.3[56] |
| TPE-CMP | 27.6 | 30.0[57] |
| HCMP-1 | 22.9 | |
| CMP-1 | 23.5 | 27.0[58] |
| TSP-1 | 28.6 | 28.1[56] |
| Tr-NPI | 25.5 | |
| CMP-3 | 22.1 | |
| Tr-PPI | 26.7 | |

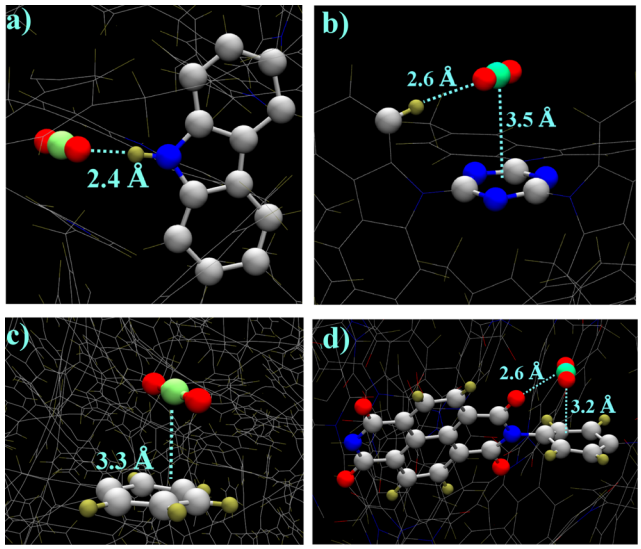


**Figure 8.** Snapshots from GCMC simulations. Possible interactions between $CO_2$ in (a) TSP-1, (b) TSP-2, (c) HCMP-1, and (d) Tr-NPI. Color scheme: Polymer atoms: C = gray, H = tan, O = red, and N = blue; $CO_2$: C = green and O = red.

## 3. CONCLUSIONS

Several amorphous microporous polymers (AMPs) have been modeled and characterized using force field based atomistic molecular dynamics simulations. The model structures were validated against experimentally determined accessible surface area, $N_2$ adsorption isotherms, powder X-ray diffraction pattern, and $CO_2$ gas uptake wherever such data were available. A crucial result from the current work is the establishment of a linear correlation between the accessible surface area of an AMP and its mass density. Unlike the former, the latter is hard to determine experimentally; thus, the relationship determined herein can aid experimentalists to estimate the density of the synthesized compound. The relationship is also a prediction from computation which requires experimental validation.

Intermolecular structural correlation between the building blocks of the compounds were investigated. Increase in the ASA of the compounds was found to be correlated to an increase in the distance between nodes. Further, the orientational ordering between near-neighbor nodes was determined


DOI: 10.1021/acs.jpcb.5b08842
J. Phys. Chem. B 2016, 120, 557−565

by calculating the angle distribution between their ring normals. AMPs with planar nodes were found to have networks in which near-neighbor nodes are oriented parallel to each other. The topology of voids in these compounds was also characterized.

Adsorption isotherms of $CO_2$ at 298 K in many AMPs were obtained through atomistic GCMC simulations within the rigid framework approximation. The absence of flexibility in the systems studied herein appears not to influence the adsorption amount of $CO_2$. We have also been able to predict the adsorption isotherms of $CO_2$ for microporous polymers which have not been measured experimentally yet. We found that microporous polymers containing nitrogen-rich building blocks show an excellent $CO_2$ uptake with a high heat of adsorption.

Specific sites of adsorption existing in microporous polymers with which $CO_2$ interacts have been identified. These include carbazole, triazine, phenyl ring, and N−H and C═O groups. The van der Waals, Lewis acid−base, hydrogen bonding, and $\pi-\pi$ interactions influence vitally the adsorption of $CO_2$ in these solids; this understanding can aid in the design of other novel architectures involving such functional groups.

## ■ ASSOCIATED CONTENT

### Supporting Information

The Supporting Information is available free of charge on the ACS Publications website at DOI: 10.1021/acs.jpcb.5b08842.

Computational details for generating structural models for AMPs, comparison between calculated PXRD patterns of model structures and experimental data (Figure S11), details of the GCMC simulation for $CO_2$ adsorption isotherms, and additional figures (PDF)

## ■ AUTHOR INFORMATION


### Corresponding Author

*Phone +91 (80) 2208 2808; Fax +91 (80) 2208 2766; e-mail bala@jncasr.ac.in.


### Notes

The authors declare no competing financial interest.

## ■ ACKNOWLEDGMENTS

S. Bonakala thanks CSIR, India, for a senior research fellowship. Prof. S. Balasubramanian thanks Sheikh Saqr Laboratory, JNCASR, for a senior fellowship. We thank Prof. Tapas Kumar Maji and his research group at JNCASR for many insightful discussions. We thank DST for support.

## ■ REFERENCES


(1) Zhang, B.; Li, G.; Yan, J.; Wang, Z. Tetraphenyladamantane-Based Microporous Polybenzimidazoles for Adsorption of Carbon Dioxide, Hydrogen, and Organic Vapors. *J. Phys. Chem. C* **2015**, *119*, 13080−13087.

(2) Rao, K. V.; Haldar, R.; Maji, T. K.; George, S. J. Porous polyimides from polycyclic aromatic linkers: Selective $CO_2$ capture and hydrogen storage. *Polymer* **2014**, *55*, 1452−1458.

(3) Liu, Q. Monodisperse Polystyrene Nanospheres with Ultrahigh Surface Area: Application for Hydrogen Storage. *Macromol. Chem. Phys.* **2010**, *211*, 1012−1017.

(4) Saleh, M.; Lee, H. M.; Kemp, K. C.; Kim, K. S. Highly Stable $CO_2/N_2$ and $CO_2/CH_4$ Selectivity in Hyper-Cross-Linked Heterocyclic Porous Polymers. *ACS Appl. Mater. Interfaces* **2014**, *6*, 7325−7333.

(5) Wu, D.; Xu, F.; Sun, B.; Fu, R.; He, H.; Matyjaszewski, K. Design and Preparation of Porous Polymers. *Chem. Rev.* **2012**, *112*, 3959−4015.

(6) Kaur, P.; Hupp, J. T.; Nguyen, S. T. Porous Organic Polymers in Catalysis: Opportunities and Challenges. *ACS Catal.* **2011**, *1*, 819−835.

(7) Farha, O. K.; Spokoyny, A. M.; Hauser, B. G.; Bae, Y.-S.; Brown, S. E.; Snurr, R. Q.; Mirkin, C. A.; Hupp, J. T. Synthesis, Properties, and Gas Separation Studies of a Robust Diimide-Based Microporous Organic Polymer. *Chem. Mater.* **2009**, *21*, 3033−3035.

(8) Weber, J.; Thomas, A. Toward Stable Interfaces in Conjugated Polymers: Microporous Poly(p-phenylene) and Poly(phenyleneethynylene) Based on a Spirobifluorene Building Block. *J. Am. Chem. Soc.* **2008**, *130*, 6334−6335.

(9) Lu, X.-L.; Zhou, T.-Y.; Wu, D.; Wen, Q.; Zhao, X.; Li, Q.; Xiang, Q.; Xu, J.-Q.; Li, Z.-T. A Triptycene-Based Porous Organic Polymer that Exhibited High Hydrogen and Carbon Dioxide Storage Capacities and Excellent $CO_2/N_2$ Selectivity. *Chin. J. Chem.* **2015**, *33*, 539−544.

(10) Shi, Q.; Sun, H.; Yang, R.; Zhu, Z.; Liang, W.; Tan, D.; Yang, B.; Li, A.; Deng, W. Synthesis of conjugated microporous polymers for gas storage and selective adsorption. *J. Mater. Sci.* **2015**, *50*, 6388−6394.

(11) Ashourirad, B.; Sekizkardes, A. K.; Altarawneh, S.; El-Kaderi, H. M. Exceptional Gas Adsorption Properties by Nitrogen-Doped Porous Carbons Derived from Benzimidazole-Linked Polymers. *Chem. Mater.* **2015**, *27*, 1349−1358.

(12) Alghunaimi, F.; Ghanem, B.; Alaslai, N.; Swaidan, R.; Litwiller, E.; Pinnau, I. Gas permeation and physical aging properties of iptycene diamine-based microporous polyimides. *J. Membr. Sci.* **2015**, *490*, 321−327.

(13) Zhang, C.; Yang, X.; Zhao, Y.; Wang, X.; Yu, M.; Jiang, J.-X. Bifunctionalized conjugated microporous polymers for carbon dioxide capture. *Polymer* **2015**, *61*, 36−41.

(14) Yang, Z.; Zhang, H.; Yu, B.; Zhao, Y.; Ma, Z.; Ji, G.; Han, B.; Liu, Z. Azo-functionalized microporous organic polymers: synthesis and applications in $CO_2$ capture and conversion. *Chem. Commun.* **2015**, *51*, 11576−11579.

(15) He, Y.; Zhu, X.; Li, Y.; Peng, C.; Hu, J.; Liu, H. Efficient $CO_2$ capture by triptycene-based microporous organic polymer with functionalized modification. *Microporous Mesoporous Mater.* **2015**, *214*, 181−187.

(16) Martin, C. F.; Stockel, E.; Clowes, R.; Adams, D. J.; Cooper, A. I.; Pis, J. J.; Rubiera, F.; Pevida, C. Hypercrosslinked organic polymer networks as potential adsorbents for pre-combustion $CO_2$ capture. *J. Mater. Chem.* **2011**, *21*, 5475−5483.

(17) Du, N.; Park, H. B.; Robertson, G. P.; Dal-Cin, M. M.; Visser, T.; Scoles, L.; Guiver, M. D. Polymer nanosieve membranes for $CO_2$-captureapplications. *Nat. Mater.* **2011**, *10*, 372−375.

(18) Eslami, H.; Kesik, M.; Karimi-Varzaneh, H. A.; Müller-Plathe, F. Sorption and diffusion of carbon dioxide and nitrogen in poly(methyl methacrylate). *J. Chem. Phys.* **2013**, *139*, 124902.

(19) Li, B.; Huang, X.; Liang, L.; Tan, B. Synthesis of uniform microporous polymer nanoparticles and their applications for hydrogen storage. *J. Mater. Chem.* **2010**, *20*, 7444−7450.

(20) Ghanem, B. S.; Msayib, K. J.; McKeown, N. B.; Harris, K. D. M.; Pan, Z.; Budd, P. M.; Butler, A.; Selbie, J.; Book, D.; Walton, A. A triptycene-based polymer of intrinsic microposity that displays enhanced surface area and hydrogen adsorption. *Chem. Commun.* **2007**, 67−69.

(21) Yuan, S.; Dorney, B.; White, D.; Kirklin, S.; Zapol, P.; Yu, L.; Liu, D.-J. Microporous polyphenylenes with tunable pore size for hydrogen storage. *Chem. Commun.* **2010**, *46*, 4547−4549.

(22) Yuan, S.; Kirklin, S.; Dorney, B.; Liu, D.-J.; Yu, L. Nanoporous Polymers Containing Stereocontorted Cores for Hydrogen Storage. *Macromolecules* **2009**, *42*, 1554−1559.

(23) Lee, J.-Y.; Wood, C. D.; Bradshaw, D.; Rosseinsky, M. J.; Cooper, A. I. Hydrogen adsorption in microporous hypercrosslinked polymers. *Chem. Commun.* **2006**, 2670−2672.

(24) Germain, J.; Hradil, J.; Fréchet, J. M. J.; Svec, F. High Surface Area Nanoporous Polymers for Reversible Hydrogen Storage. *Chem. Mater.* **2006**, *18*, 4430−4435.

(25) Wood, C. D.; Tan, B.; Trewin, A.; Niu, H.; Bradshaw, D.; Rosseinsky, M. J.; Khimyak, Y. Z.; Campbell, N. L.; Kirk, R.; Stöckel,

E.; Cooper, A. I. Hydrogen Storage in Microporous Hypercrosslinked Organic Polymer Networks. *Chem. Mater.* **2007**, *19*, 2034−2048.
(26) Wood, C. D.; Tan, B.; Trewin, A.; Su, F.; Rosseinsky, M. J.; Bradshaw, D.; Sun, Y.; Zhou, L.; Cooper, A. I. Microporous Organic Polymers for Methane Storage. *Adv. Mater.* **2008**, *20*, 1916−1921.
(27) Furukawa, H.; Yaghi, O. M. Storage of Hydrogen, Methane, and Carbon Dioxide in Highly Porous Covalent Organic Frameworks for Clean Energy Applications. *J. Am. Chem. Soc.* **2009**, *131*, 8875−8883.
(28) Schwab, M. G.; Lennert, A.; Pahnke, J.; Jonschker, G.; Koch, M.; Senkovska, I.; Rehahn, M.; Kaskel, S. Nanoporous copolymer networks through multiple Friedel-Crafts-alkylation-studies on hydrogen and methane storage. *J. Mater. Chem.* **2011**, *21*, 2131−2135.
(29) Uemura, K.; Komagawa, Y.; Yamasaki, Y.; Kita, H. Characterization of organic solvents adsorption/desorption on hydrophobic porous coordination polymers and their micro-crystals aggregation on mullite support. *Desalination* **2008**, *234*, 1−8.
(30) Kaleeswaran, D.; Vishnoi, P.; Murugavel, R. [3 + 3] Imine and [small beta]-ketoenamine tethered fluorescent covalent-organic frameworks for $CO_2$ uptake and nitroaromatic sensing. *J. Mater. Chem. C* **2015**, *3*, 7159−717.
(31) Côté, A. P.; Benin, A. I.; Ockwig, N. W.; O'Keeffe, M.; Matzger, A. J.; Yaghi, O. M. Porous, Crystalline, Covalent Organic Frameworks. *Science* **2005**, *310*, 1166−1170.
(32) El-Kaderi, H. M.; Hunt, J. R.; Mendoza-Cortés, J. L.; Côté, A. P.; Taylor, R. E.; O'Keeffe, M.; Yaghi, O. M. Designed Synthesis of 3D Covalent Organic Frameworks. *Science* **2007**, *316*, 268−272.
(33) Han, S. S.; Furukawa, H.; Yaghi, O. M.; Goddard, W. A. Covalent Organic Frameworks as Exceptional Hydrogen Storage Materials. *J. Am. Chem. Soc.* **2008**, *130*, 11580−11581.
(34) McKeown, N. B.; Gahnem, B.; Msayib, K. J.; Budd, P. M.; Tattershall, C. E.; Mahmood, K.; Tan, S.; Book, D.; Langmi, H. W.; Walton, A. Towards Polymer-Based Hydrogen Storage Materials: Engineering Ultramicroporous Cavities within Polymers of Intrinsic Microporosity. *Angew. Chem., Int. Ed.* **2006**, *45*, 1804−1807.
(35) McKeown, N. B.; Budd, P. M.; Msayib, K. J.; Ghanem, B. S.; Kingston, H. J.; Tattershall, C. E.; Makhseed, S.; Reynolds, K. J.; Fritsch, D. Polymers of Intrinsic Microporosity (PIMs): Bridging the Void between Microporous and Polymeric Materials. *Chem. - Eur. J.* **2005**, *11*, 2610−2620.
(36) Swaidan, R. J.; Ghanem, B.; Swaidan, R.; Litwiller, E.; Pinnau, I. Pure- and mixed-gas propylene/propane permeation properties of spiro- and triptycene-based microporous polyimides. *J. Membr. Sci.* **2015**, *492*, 116−122.
(37) Du, N.; Robertson, G. P.; Song, J.; Pinnau, I.; Thomas, S.; Guiver, M. D. Polymers of Intrinsic Microporosity Containing Trifluoromethyl and Phenylsulfone Groups as Materials for Membrane Gas Separation. *Macromolecules* **2008**, *41*, 9656−9662.
(38) Tan, L.; Li, B.; Yang, X.; Wang, W.; Tan, B. Knitting hypercrosslinked conjugated microporous polymers with external crosslinker. *Polymer* **2015**, *70*, 336−342.
(39) Zhuang, X.; Gehrig, D.; Forler, N.; Liang, H.; Wagner, M.; Hansen, M. R.; Laquai, F.; Zhang, F.; Feng, X. Conjugated Microporous Polymers with Dimensionality-Controlled Heterostructures for Green Energy Devices. *Adv. Mater.* **2015**, *27*, 3789−3796.
(40) Dawson, R.; Su, F.; Niu, H.; Wood, C. D.; Jones, J. T. A.; Khimyak, Y. Z.; Cooper, A. I. Mesoporous Poly(phenylenevinylene) Networks. *Macromolecules* **2008**, *41*, 1591−1593.
(41) Errahali, M.; Gatti, G.; Tei, L.; Paul, G.; Rolla, G. A.; Canti, L.; Fraccarollo, A.; Cossi, M.; Comotti, A.; Sozzani, P.; Marchese, L. Microporous Hyper-Cross-Linked Aromatic Polymers Designed for Methane and Carbon Dioxide Adsorption. *J. Phys. Chem. C* **2014**, *118*, 28699−28710.
(42) Ma, H.; Ren, H.; Zou, X.; Meng, S.; Sun, F.; Zhu, G. Post-metalation of porous aromatic frameworks for highly efficient carbon capture from $CO_2$ + $N_2$ and $CH_4$ + $N_2$ mixtures. *Polym. Chem.* **2014**, *5*, 144−152.
(43) Watkins, M. B.; Shevlin, S. A.; Sokol, A. A.; Slater, B.; Catlow, C. R. A.; Woodley, S. M. Bubbles and microporous frameworks of silicon carbide. *Phys. Chem. Chem. Phys.* **2009**, *11*, 3186−3200.
(44) Reece, C.; Willock, D. J.; Trewin, A. Modelling analysis of the structure and porosity of covalent triazine-based frameworks. *Phys. Chem. Chem. Phys.* **2015**, *17*, 817−823.
(45) Zhou, X.; Huang, J.; Barr, K. W.; Lin, Z.; Maya, F.; Abbott, L. J.; Colina, C. M.; Svec, F.; Turner, S. R. Nanoporous hypercrosslinked polymers containing Tg enhancing comonomers. *Polymer* **2015**, *59*, 42−48.
(46) Hart, K. E.; Colina, C. M. Ionomers of Intrinsic Microporosity: In Silico Development of Ionic-Functionalized Gas-Separation Membranes. *Langmuir* **2014**, *30*, 12039−12048.
(47) Jiang, S.; Jelfs, K. E.; Holden, D.; Hasell, T.; Chong, S. Y.; Haranczyk, M.; Trewin, A.; Cooper, A. I. Molecular Dynamics Simulations of Gas Selectivity in Amorphous Porous Molecular Solids. *J. Am. Chem. Soc.* **2013**, *135*, 17818−17830.
(48) Abbott, L. J.; Colina, C. M. Atomistic Structure Generation and Gas Adsorption Simulations of Microporous Polymer Networks. *Macromolecules* **2011**, *44*, 4511−4519.
(49) Nawaz, S.; Redhead, M.; Mantovani, G.; Alexander, C.; Bosquillon, C.; Carbone, P. Interactions of PEO-PPO-PEO block copolymers with lipid membranes: a computational and experimental study linking membrane lysis with polymer structure. *Soft Matter* **2012**, *8*, 6744−6754.
(50) Trewin, A.; Willock, D. J.; Cooper, A. I. Atomistic Simulation of Micropore Structure, Surface Area, and Gas Sorption Properties for Amorphous Microporous Polymer Networks. *J. Phys. Chem. C* **2008**, *112*, 20549−20559.
(51) Li, A.; Sun, H.-X.; Tan, D.-Z.; Fan, W.-J.; Wen, S.-H.; Qing, X.-J.; Li, G.-X.; Li, S.-Y.; Deng, W.-Q. Superhydrophobic conjugated microporous polymers for separation and adsorption. *Energy Environ. Sci.* **2011**, *4*, 2062−2065.
(52) Dawson, R.; Laybourn, A.; Clowes, R.; Khimyak, Y. Z.; Adams, D. J.; Cooper, A. I. Functionalized Conjugated Microporous Polymers. *Macromolecules* **2009**, *42*, 8809−8816.
(53) Kuhn, P.; Kruger, K.; Thomas, A.; Antonietti, M. "Everything is surface": tunable polymer organic frameworks with ultrahigh dye sorption capacity. *Chem. Commun.* **2008**, 5815−5817.
(54) Zhang, Y.; Wei, S.; Liu, F.; Du, Y.; Liu, S.; Ji, Y.; Yokoi, T.; Tatsumi, T.; Xiao, F.-S. Superhydrophobic nanoporous polymers as efficient adsorbents for organic compounds. *Nano Today* **2009**, *4*, 135−142.
(55) Rao, K. V.; Mohapatra, S.; Maji, T. K.; George, S. J. Guest-Responsive Reversible Swelling and Enhanced Fluorescence in a Super-Absorbent, Dynamic Microporous Polymer. *Chem. - Eur. J.* **2012**, *18*, 4505−4509.
(56) Zhu, X.; Mahurin, S. M.; An, S.-H.; Do-Thanh, C.-L.; Tian, C.; Li, Y.; Gill, L. W.; Hagaman, E. W.; Bian, Z.; Zhou, J.-H.; Hu, J.; et al. Efficient $CO_2$ capture by a task-specific porous organic polymer bifunctionalized with carbazole and triazine groups. *Chem. Commun.* **2014**, *50*, 7933−7936.
(57) Suresh, V. M.; Bonakala, S.; Roy, S.; Balasubramanian, S.; Maji, T. K. Synthesis, Characterization, and Modeling of a Functional Conjugated Microporous Polymer: $CO_2$ Storage and Light Harvesting. *J. Phys. Chem. C* **2014**, *118*, 24369−24376.
(58) Dawson, R.; Adams, D. J.; Cooper, A. I. Chemical tuning of $CO_2$ sorption in robust nanoporous organic polymers. *Chem. Sci.* **2011**, *2*, 1173−1177.
(59) Jiang, J.-X.; Su, F.; Trewin, A.; Wood, C. D.; Niu, H.; Jones, J. T. A.; Khimyak, Y. Z.; Cooper, A. I. Synthetic Control of the Pore Dimension and Surface Area in Conjugated Microporous Polymer and Copolymer Networks. *J. Am. Chem. Soc.* **2008**, *130*, 7710−7720.
(60) Jiang, J.-X.; Su, F.; Trewin, A.; Wood, C.; Campbell, N.; Niu, H.; Dickinson, C.; Ganin, A.; Rosseinsky, M.; Khimyak, Y.; Cooper, A. Conjugated Microporous Poly(aryleneethynylene) Networks. *Angew. Chem., Int. Ed.* **2007**, *46*, 8574−8578.
(61) Düren, T.; Millange, F.; Férey, G.; Walton, K. S.; Snurr, R. Q. Calculating Geometric Surface Areas as a Characterization Tool for Metal-Organic Frameworks. *J. Phys. Chem. C* **2007**, *111*, 15350−15356.


DOI: 10.1021/acs.jpcb.5b08842
*J. Phys. Chem. B* 2016, 120, 557−565

(62) Brunauer, S.; Emmett, P. H.; Teller, E. Adsorption of Gases in Multimolecular Layers. *J. Am. Chem. Soc.* **1938**, *60*, 309−319.
(63) Düren, T.; Sarkisov, L.; Snurr, R. Q. Research Section Calculating the accessible surface area for non-orthorhombic unit cells, 2007.
(64) Zhang, K.; Vobecka, Z.; Tauer, K.; Antonietti, M.; Vilela, F. π-Conjugated polyHIPEs as highly efficient and reusable heterogeneous photosensitizers. *Chem. Commun.* **2013**, *49*, 11158−11160.
(65) Urakami, H.; Zhang, K.; Vilela, F. Modification of conjugated microporous poly-benzothiadiazole for photosensitized singlet oxygen generation in water. *Chem. Commun.* **2013**, *49*, 2353−2355.
(66) Rao, K. V.; Haldar, R.; Kulkarni, C.; Maji, T. K.; George, S. J. Perylene Based Porous Polyimides: Tunable, High Surface Area with Tetrahedral and Pyramidal Monomers. *Chem. Mater.* **2012**, *24*, 969−971.
(67) Macrae, C. F.; Edgington, P. R.; McCabe, P.; Pidcock, E.; Shields, G. P.; Taylor, R.; Towler, M.; van de Streek, J. Mercury: visualization and analysis of crystal structures. *J. Appl. Crystallogr.* **2006**, *39*, 453−457.
(68) Jedlovszky, P. Orientational correlation in liquid and amorphous carbon tetrachloride: A reverse Monte Carlo study. *J. Chem. Phys.* **1997**, *107*, 7433.
(69) Wang, Z.; Zhang, B.; Yu, H.; Li, G.; Bao, Y. Synthetic control of network topology and pore structure in microporous polyimides based on triangular triphenylbenzene and triphenylamine units. *Soft Matter* **2011**, *7*, 5723−5730.
(70) Trewin, A.; Cooper, A. I. Predicting microporous crystalline polyimides. *CrystEngComm* **2009**, *11*, 1819−1822.
(71) Bonakala, S.; Balasubramanian, S. Modelling Gas Adsorption in Porous Solids: Roles of Surface Chemistry and Pore Architecture. *J. Chem. Sci.* **2015**, *127*, 1687−1699.
(72) Auerbach, S. M.; Metiu, H. I. Modeling orientational randomization in zeolites: A new probe of intracage mobility, diffusion and cation disorder. *J. Chem. Phys.* **1997**, *106*, 2893−2905.
(73) Hu, J.-X.; Shang, H.; Wang, J.-G.; Luo, L.; Xiao, Q.; Zhong, Y.-J.; Zhu, W.-D. Highly Enhanced Selectivity and Easy Regeneration for the Separation of $CO_2$ over $N_2$ on Melamine-Based Microporous Organic Polymers. *Ind. Eng. Chem. Res.* **2014**, *53*, 11828−11837.
(74) Zhu, X.; Do-Thanh, C.-L.; Murdock, C. R.; Nelson, K. M.; Tian, C.; Brown, S.; Mahurin, S. M.; Jenkins, D. M.; Hu, J.; Zhao, B.; Liu, H.; et al. Efficient $CO_2$ Capture by a 3D Porous Polymer Derived from Tröger's Base. *ACS Macro Lett.* **2013**, *2*, 660−663.
(75) Zhao, Y.; Yao, K. X.; Teng, B.; Zhang, T.; Han, Y. A perfluorinated covalent triazine-based framework for highly selective and water-tolerant $CO_2$ capture. *Energy Environ. Sci.* **2013**, *6*, 3684−3692.
(76) Rabbani, M. G.; El-Kaderi, H. M. Synthesis and Characterization of Porous Benzimidazole-Linked Polymers and Their Performance in Small Gas Storage and Selective Uptake. *Chem. Mater.* **2012**, *24*, 1511−1517.
(77) Patel, H. A.; Hyun, J. S.; Park, J.; Chen, D. P.; Jung, Y.; Yavuz, C. T.; Coskun, A. Unprecedented high-temperature $CO_2$ selectivity in $N_2$-phobic nanoporous covalent organic polymers. *Nat. Commun.* **2013**, *4*, 1357.
(78) Luo, Y.; Li, B.; Wang, W.; Wu, K.; Tan, B. Hypercrosslinked Aromatic Heterocyclic Microporous Polymers: A New Class of Highly Selective $CO_2$ Capturing Materials. *Adv. Mater.* **2012**, *24*, 5703−5707.
(79) Nicholson, D.; Parsonage, N. G. *Computer Simulation and the Statistical Mechanics of Adsorption*; Academic Press: 1982.
(80) Derewenda, Z. S.; Lee, L.; Derewenda, U. The Occurence of C-H···O Hydrogen Bonds in Proteins. *J. Mol. Biol.* **1995**, *252*, 248−262.
(81) Gautham, R. D.; Thomas, S. *The Weak Hydrogen Bond: In Structural Chemistry and Biology*; Oxford University Press: 2001.
(82) Hunter, C. A.; Sanders, J. K. M. The nature of π-π interactions. *J. Am. Chem. Soc.* **1990**, *112*, 5525−5534.
(83) Baburin, I. A.; Blatov, V. A.; Carlucci, L.; Ciani, G.; Proserpio, D. M. Interpenetrated three-dimensional hydrogen-bonded networks from metal-organic molecular and one- or two-dimensional polymeric motifs. *CrystEngComm* **2008**, *10*, 1822−1838.


DOI: 10.1021/acs.jpcb.5b08842
*J. Phys. Chem. B* 2016, 120, 557−565